Chemistry & Biology
Article

Structural Basis for Specific, High-Affinity Tetracycline Binding by an In Vitro Evolved Aptamer and Artificial Riboswitch

Hong Xiao,[1,2] Thomas E. Edwards,[2,3] and Adrian R. Ferré-D'Amaré[1,2,*]
[1]Howard Hughes Medical Institute
[2]Division of Basic Sciences
Fred Hutchinson Cancer Research Center,1100 Fairview Avenue North, Seattle, WA 98109-1024, USA
[3]Present address: deCODE Biostructures, 7869 Northeast Day Road West, Bainbridge Island, WA 98110 USA
*Correspondence: aferre@fhcrc.org
DOI 10.1016/j.chembiol.2008.09.004

SUMMARY

The tetracycline aptamer is an in vitro selected RNA that binds to the antibiotic with the highest known affinity of an artificial RNA for a small molecule (K_d ~0.8 nM). It is one of few aptamers known to be capable of modulating gene expression in vivo. The 2.2 Å resolution cocrystal structure of the aptamer reveals a pseudoknot-like fold formed by tertiary interactions between an 11 nucleotide loop and the minor groove of an irregular helix. Tetracycline binds within this interface as a magnesium ion chelate. The structure, together with previous biochemical and biophysical data, indicates that the aptamer undergoes localized folding concomitant with tetracycline binding. The three-helix junction, h-shaped architecture of this artificial RNA is more complex than those of most aptamers and is reminiscent of the structures of some natural riboswitches.

INTRODUCTION

Aptamers are artificially evolved RNAs selected in vitro to bind to other molecules (Ellington and Szostak, 1990). Numerous aptamers have been discovered that bind to ligands as diverse as metal ions, small organic molecules, nucleic acids, and proteins. Several of them have been characterized biochemically and structurally (reviewed in Feigon et al., 1996; Hermann and Patel, 2000; Wilson and Szostak, 1999). Aptamers that bind to small organic molecules have been of interest both to elucidate the structural basis of molecular recognition by RNA, and as part of efforts to develop biotechnological tools such as affinity tags, biosensors, and small-molecule responsive enzymes (Lorenz and Schroeder, 2006). In recent years, it was discovered that archaea, bacteria, and eukarya employ highly structured mRNA domains to bind directly to intracellular metabolites (reviewed in Edwards et al., 2007). Binding of these noncoding mRNA domains, called riboswitches, to their cognate effectors results in a change in transcription, translation, or posttranscriptional processing of the mRNA of which they are part. By analogy with the in vitro selected RNAs, the moiety of a natural riboswitch that suffices for specific binding to its effector metabolite has been referred to as its "aptamer domain."

The tetracycline aptamer was identified by Schroeder and coworkers through in vitro selection from a pool of RNAs containing 74 nucleotides (nt) of random sequence (Berens et al., 2001). RNAs were bound to an affinity column with immobilized tetracycline, and molecules that were eluted specifically with tetracycline were amplified and used in further rounds of selection. Biochemical characterization of cb28, one of the resulting tetracycline-binding RNAs, was used to guide the design of a 60 nt "cb28 minimer" (Berens et al., 2001). This compact tetracycline aptamer was found to bind to its ligand with a dissociation constant of ~0.8 nM, which is three orders of magnitude tighter than binding of the antibiotic to the 30S subunit of the bacterial ribosome, tighter than any other known aptamer-small molecule interaction (Müller et al., 2006), and similar to the tightest known natural riboswitch-small molecule interaction (Welz and Breaker, 2007).

Previous crystallographic and NMR characterization of aptamers that recognize small molecules has revealed a preponderance of structures consisting of single helical stacks with an irregularly structured segment that encapsulates the ligand at the junction of two helices (Feigon et al., 1996; Hermann and Patel, 2000; Wilson and Szostak, 1999). In contrast, the tetracycline aptamer comprises three helices, one of which is closed by a long loop. Chemical and enzymatic probing experiments suggest that this stem-loop forms the antibiotic binding site by associating with a distant segment that connects the other two helices (Berens et al., 2001; Hanson et al., 2005). Such a binding site, resulting from long-range (tertiary) contacts, would be different from those of most aptamers, but is reminiscent of the metabolite binding sites of several naturally occurring riboswitches (reviewed in Edwards et al., 2007). Indeed, Suess and coworkers have successfully employed the tetracycline aptamer as an artificial riboswitch (reviewed in Suess and Weigand, 2008). By introducing the aptamer into two introns of a yeast mRNA, they achieved 32-fold tetracycline-mediated repression of gene expression in vivo (Weigand and Suess, 2007). This compares favorably with the best artificial riboswitches, and is within a factor of three of some natural riboswitches (Lynch et al., 2007).

We have now determined the cocrystal structure of the cb28 minimer in order to elucidate the chemical underpinnings for high-affinity and high-specificity binding of tetracycline by this

RNA. Our work also provides a structural framework for rationalizing the considerable body of biochemical and biophysical characterization previously carried out on this system, and serves as a starting point in further engineering of this artificial riboswitch. The structure lays bare the mechanism of tetracycline recognition by this aptamer, and suggests the molecular nature of a localized RNA conformational rearrangement that accompanies antibiotic binding. Moreover, because structures of tetracycline bound to its antibacterial target, the 30S ribosome, as well as to the tetracycline repressor (TetR) protein have previously been determined, we have been able to compare and contrast different ways in which RNAs and proteins recognize this widely employed antibiotic.

RESULTS

Crystallization and Structure Determination

The cb28 minimer of Berens et al. (2001) comprises three helices, P1, P2, and P3, with loops P2 and P3 closing the distal ends of the latter two (Figure 1A). In the course of minimizing cb28, these authors replaced the original 16 nt closing the P2 helix with a UUCG tetraloop. Similarly, P1 resulted from deletion of 19 residues. These and other analyses indicate that the distal ends of P1 and P2 are functionally dispensable. In contrast, L3 was found to be essential for tetracycline binding (Berens et al., 2001; Hanson et al., 2005). In order to facilitate crystallization and structure determination, we generated circularly permuted aptamer constructs in which the distal end of P1 was closed with the U1A binding site (Ferré-D'Amaré et al., 1998b), and L2 was deleted (Figure 1B). The U1A complex of this permuted aptamer binds the antibiotic with an affinity that is comparable to that of the wild-type aptamer (see Figure S1 available online). As is conventional (Ferré-D'Amaré and Doudna, 2000b; Ferré-D'Amaré et al., 1998a), we generated a panel of crystallization candidate RNAs by varying the number of spacer base pairs between the U1A binding site and P1, and the number and sequence of P2 terminal nucleotides. A circularly permuted 65 nt tetracycline aptamer construct produced well-ordered cocrystals when complexed with selenomethionyl U1A RNA-binding domain (RBD) and 7-chlorotetracycline. Previously, it was shown that presence of a chlorine at position 7 of tetracycline (Figure 1C) slightly increases affinity of the antibiotic for the cb28 minimer (K_d = 0.6 versus 0.8 nM; Müller et al., 2006). The structure was solved by the multiwavelength anomalous dispersion (MAD) method, and refined against diffraction data extending to 2.2 Å resolution. The current crystallographic model has a free R factor of 26.3% and a mean precision of 0.2 Å (Table 1; Experimental Procedures). The congruence of our structure of the circularly permuted RNA with previous biochemical data on the tetracycline aptamer (below) and the similarity in the affinity for the antibiotic of the wild-type and permuted RNAs suggest that engineering of the RNA construct for crystallization has not drastically altered the mode of interaction of the aptamer and antibiotic.

Overall Structure

The tetracycline aptamer fold resembles an inverted "h," with the antibiotic binding site at the junction of two helical stacks (Figure 1; Figure S2). Helices P1 and P3, and loop L3 stack on each other. Helix P2 stacks on an irregular helix formed by association of joining regions J1/2 and J2/3. The three-dimensional structure of the ligand-bound state of the aptamer results from a series of tertiary interactions between the 11 nt L3 loop and the minor groove face of the irregular helix. L3 nucleotides 55–57 form nonstandard pairs with nucleotides from J1/2 and J2/3. Thus, the fold of the aptamer comprises a noncanonical pseudoknot (a canonical pseudoknot results from Watson-Crick pairing of nucleotides from the loop of a stem-loop and nucleotides outside the stem-loop; Pleij, 1990). In addition to tertiary RNA interactions, the structure appears to be stabilized by the bound antibiotic, a series of tightly bound divalent cations, and a network of ordered water molecules.

The core of the aptamer structure is formed by an irregular triplex (Figures 2A and 2B) resulting from close apposition of J1/2, J2/3, and three L3 nucleotides. In this region of the RNA, the backbones of J2/3 and L3 run in the same direction, whereas J1/2 is antiparallel. At the transition from P1 (gray in Figures 1E and 2) to J1/2 (magenta), the RNA chain makes an abrupt turn, such that whereas residue 6 at the top of helix P1 is in a standard A-form helical environment, residue 7 is nearly perpendicular, and one face of its adenine base is completely unstacked and solvent exposed (Figures 1D and 2A). Neither A7 nor A8 participate in base pairing, but they stack underneath the helical stack of residues from J2/3, which is running with the opposite polarity (Figures 2A and 2B). Like A7, A9 is unstacked on its bottom face, and forms part of a coplanar base triple. It makes a *cis* Hoogsteen edge to Watson-Crick base pair with A44, and simultaneously makes a *trans* Watson-Crick pair with A55. The *trans* orientation of this pair results from the parallel direction of the backbones of A9 and A55. This base triple stacks on a *trans* Watson-Crick pair formed by C10 and C56. The two cytosine bases share three hydrogen bonds, with their N3 groups separated by 2.6 Å. This implies that these imine nitrogen atoms are partially protonated.

Close packing of the aptamer core is facilitated by interdigitation of G57 from L3 between G43 and A44 of J2/3 (Figure 2B). G57 stacks between these two bases, and also makes a hydrogen bond to a nonbridging phosphate oxygen of A44. In turn, G43 makes a ribose zipper-type interaction between its 2′-OH and the N3 and 2′-OH of G57. A11 from J1/2 protrudes deeply into the minor groove, and its N1 hydrogen bonds to the 2′-OH of C56. The Hoogsteen face of G57 makes one hydrogen bond each with the bases of C10 (thus forming a second base triple) and A11. This bifurcated base pairing and the interdigitation together have the result that the triplex comprises five nucleotides in the continuous J1/2 strand (A9–A13) and only four in the opposite composite strand (A42–A44 from J2/3, and G57 from L3). Toward the 3′ end of J1/2, the minor groove is stretched by a single-hydrogen-bond base pair formed between U12 and G43. This pair appears to be stabilized in addition by a water-mediated Watson-Crick face interaction. Finally, A13 and A42 share a single hydrogen bond between their Watson-Crick faces.

The base of the L3 loop is closed by a single-hydrogen-bond pair between A49 and C59 (their N1 and N4 atoms, respectively, are 2.8 Å apart; Figure 2A). A50 and A58 stack on this pair, but they are too distant from each other to hydrogen bond (their closest approach, between N3 of A50 and N6 of A58, is 4.1 Å). Nucleotides G51 and A52 stack on each other and on the 5′ side of the

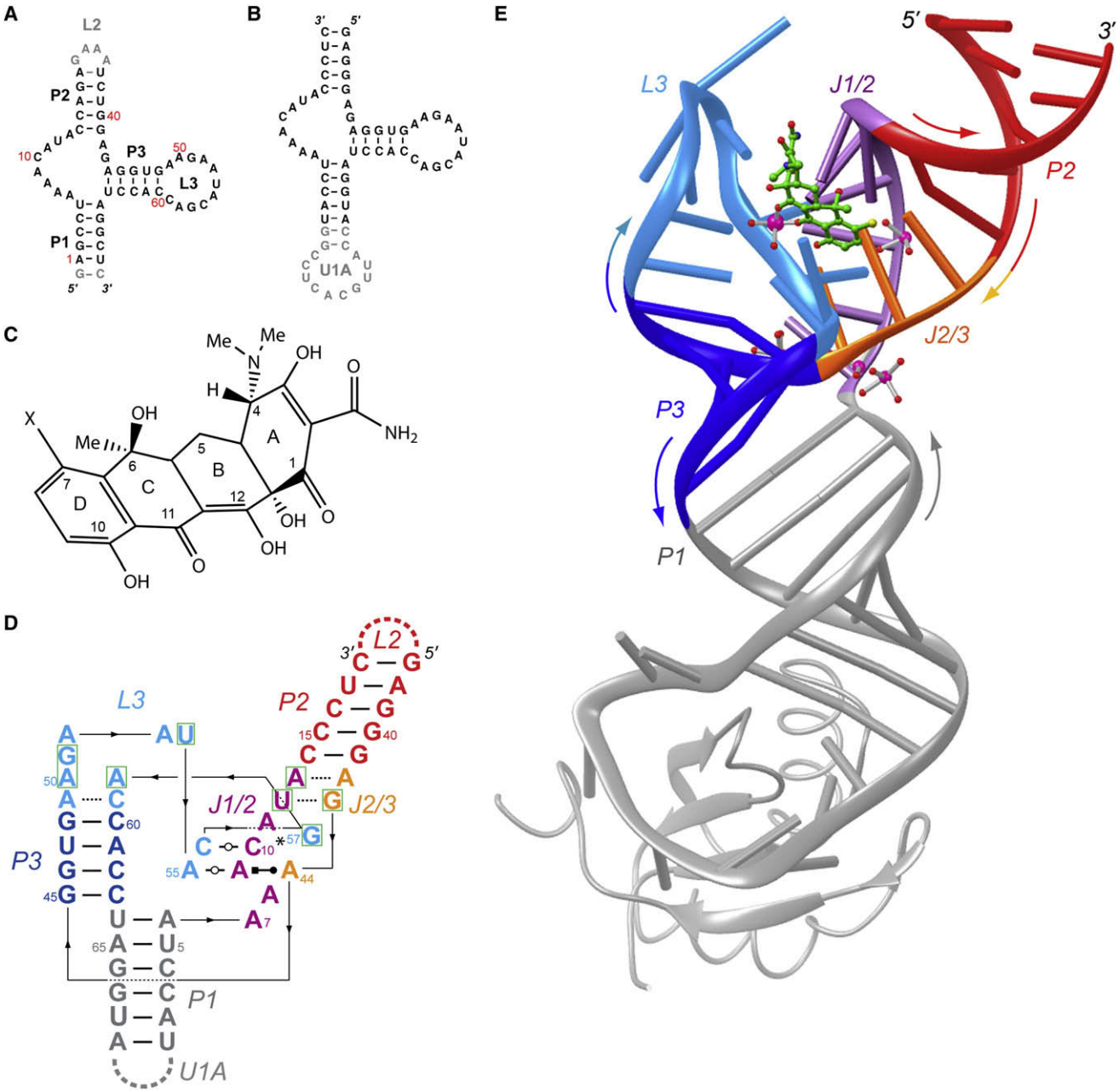

Figure 1. Overall Structure of the Tetracycline Aptamer

(A) Sequence of a wild-type connectivity tetracycline aptamer. Residue numbers correspond to those of the constructs of Hanson et al. (2005) and Müller et al. (2006). Gray nucleotides are functionally dispensable.

(B) Sequence of the circularly permuted crystallization construct. Note deletion of loop L2, and introduction of a U1A protein binding site capping paired region P1.

(C) Chemical structure of tetracycline, numbered conventionally. X is hydrogen or chlorine, for tetracycline and 7-chlorotetracycline, respectively.

(D) Schematic secondary structure of the tetracycline-bound conformation of the aptamer. Nucleotides that form the antibiotic binding site are boxed in green. Thin lines with embedded arrowheads depict connectivity. Watson-Crick and single-hydrogen-bond pairs are indicated by thin and dashed lines, respectively. Noncanonical base-pair symbols are those of Leontis and Westhof (2001). Asterisk indicates that the base of G57 makes single hydrogen bonds with the bases of both C10 and A11.

(E) Cartoon representation of the tetracycline aptamer (color coded as in [D]) in complex with 7-chlorotetracycline (green stick figure) and U1A. Selected well-ordered magnesium ions and their solvation waters (magenta and red spheres, respectively) are shown. Colored arrows denote chain direction.

loop in a manner not dissimilar from that seen in GNRA tetraloops (Figure 2C). However, the next two nucleotides adopt atypical conformations. A53 is unstacked and projects toward the back of the loop. The base of U54 packs against the loop from the rear, and hydrogen bonds to the base and to the sugar of G51. This is made possible by a pronounced C3′-*exo*

Table 1. Crystallographic Statistics

	Remote	Inflection	Peak
Diffraction Data			
Wavelength (Å)	0.9570	0.9797	0.9795
Resolution (Å)[a]	30.0–2.2 (2.3–2.2)	30.0–2.3 (2.4–2.3)	30–2.5 (2.6–2.5)
R_{merge} (%)[a]	8.0 (53.2)	7.4 (55.1)	7.8 (56.2)
$< I >/< \sigma(I) >$[a]	37.6 (3.8)	36.6 (3.8)	36.4 (4.1)
Completeness (%)[a]	99.1 (99.9)	99.1 (99.8)	98.9 (99.7)
Redundancy[a]	9.5 (9.8)	9.5 (9.7)	9.5 (9.7)
Phasing			
Phasing power			
Iso (acentrics)	n/a	3.56	2.90
Ano (acentrics)	1.38	3.78	3.29
R_{cullis} (%) Ano	72.6	49.4	45.6
Mean overall figure of merit	0.53		
Refinement			
Number of reflections[b]	19,015 (2,156)		
R_{work}/R_{free} (%)	21.6/26.3		
Number of atoms			
RNA	1,380		
Protein	728		
7-Cl-tetracycline	33		
Ion	12		
Water	146		
Mean B factors (Å^2)			
RNA	52.5		
Protein	42.2		
7-Cl-tetracycline	68.5		
Ion	61.3		
Water	48.4		
Root-mean-square deviations			
Bond lengths (Å)	0.012		
Bond angles (°)	1.963		
REFMAC coordinate	0.24 (0.21)		
Precision (Å)[b]			
PDB ID code	3EGZ		

n/a, not applicable.
[a] Values in parentheses are for the highest resolution shell.
[b] Values in parentheses are for the crossvalidation set.

puckering of the ribose of U54. The next three nucleotides project away from L3 and form part of the core triplex, as described above. The peculiar conformation of L3 is facilitated by a series of direct and water-mediated hydrogen bonds, as well as magnesium ion coordination (Figure 2C).

Tetracycline Binding Pocket

Binding to the aptamer buries 425 Å^2 out of the 621 Å^2 total solvent-accessible surface area of 7-chlorotetracycline. The binding site is formed by the minor grooves of L3 and the J1/2 and J2/3 helix. As has previously been observed in its complexes with the 30S ribosomal subunit (Brodersen et al., 2000) and with the TetR protein (Hinrichs et al., 1994), the antibiotic binds to the aptamer RNA as a magnesium ion chelate. The ketoenolate oxygens at positions 11 and 12 of tetracycline (Figure 1C) provide two of the six inner-sphere ligands of the octahedrally coordinated magnesium ion. The ketoenolate face of chlorotetracycline is deeply buried in the RNA. In contrast, the edge of the antibiotic that bears the dimethylamine group (position 4) and the chlorine (position 7) is exposed to solvent (Figures 3A and 3B).

The tetracycline aptamer recognizes its ligand employing a variety of interactions. The α (lower, in the views in Figure 3) face of the conjugated rings C and D of the antibiotic (Figure 1C) stacks on the purine base of A58. The strongest feature in the unbiased residual electron density map (Figure 3C) is the deeply buried magnesium ion coordinated to the antibiotic. In addition to the two oxygen ligands provided by 7-chlorotetracycline, the metal ion makes an inner-sphere coordination with the *pro*-R_P nonbridging phosphate oxygen of G57. Two water molecules that make additional inner-sphere coordinations with the magnesium ion are clearly visible. At the current resolution limit, there is no electron density for the sixth ligand, but space is present in the binding pocket for a third water molecule to occupy this axial position on the β side of tetracycline. A50 and A58 indirectly recognize the magnesium ion by making three hydrogen bonds to two of its coordination waters. In addition, the exocyclic amine of A50 appears to stabilize the backbone of G57 by making a water-mediated hydrogen bond with its *pro*-S_P phosphate oxygen. RNA bases do not stack on the upper (β) face of the antibiotic. Instead, A13 makes three hydrogen bonds with functional groups on this face. The N3 and 2′-OH of the nucleotide both hydrogen bond to the 6β-OH group of tetracycline, and its O4′ ribose oxygen makes a hydrogen bond with the nitrogen of the amide group of the antibiotic. This amide group is also in van der Waals contact with the base of U54 (Figures 3B and 3C).

RNA Hydration and Counterions

A prominent feature of the tetracycline binding site of the aptamer is the presence of numerous well-ordered water molecules directly below the antibiotic in the major groove of L3 (Figure 4A; Figure S3). These waters have crystallographic B factors comparable to those of the RNA atoms. At the current resolution (2.2 Å), the number of crystallographically observed water molecules is most likely an underestimate of the waters trapped in the major groove. There are additional ordered water molecules in the major groove of L3 above the antibiotic. Thus, despite the large fraction of its surface area buried by the RNA, the antibiotic is bound in hydrated form.

The L3 major groove waters delineate a continuous path leading from the α face of the antibiotic to an entry at the junction of the major grooves of P3 and the constriction formed by the close approach of the backbones of J1/2 and J2/3. Three particularly well ordered magnesium ions lie across this portal (Figure 4B; Figure S3). The first of these (marked * in Figure 4) is fully hydrated, and makes at least eight hydrogen bonds to the RNA through its inner-sphere, octahedrally coordinated water molecules. Additional hydrogen bonds to the RNA through outer-sphere coordination water molecules are also present. Two partially desolvated magnesium ions track the narrow groove formed by the closely apposed backbones of J1/2 and J2/3.

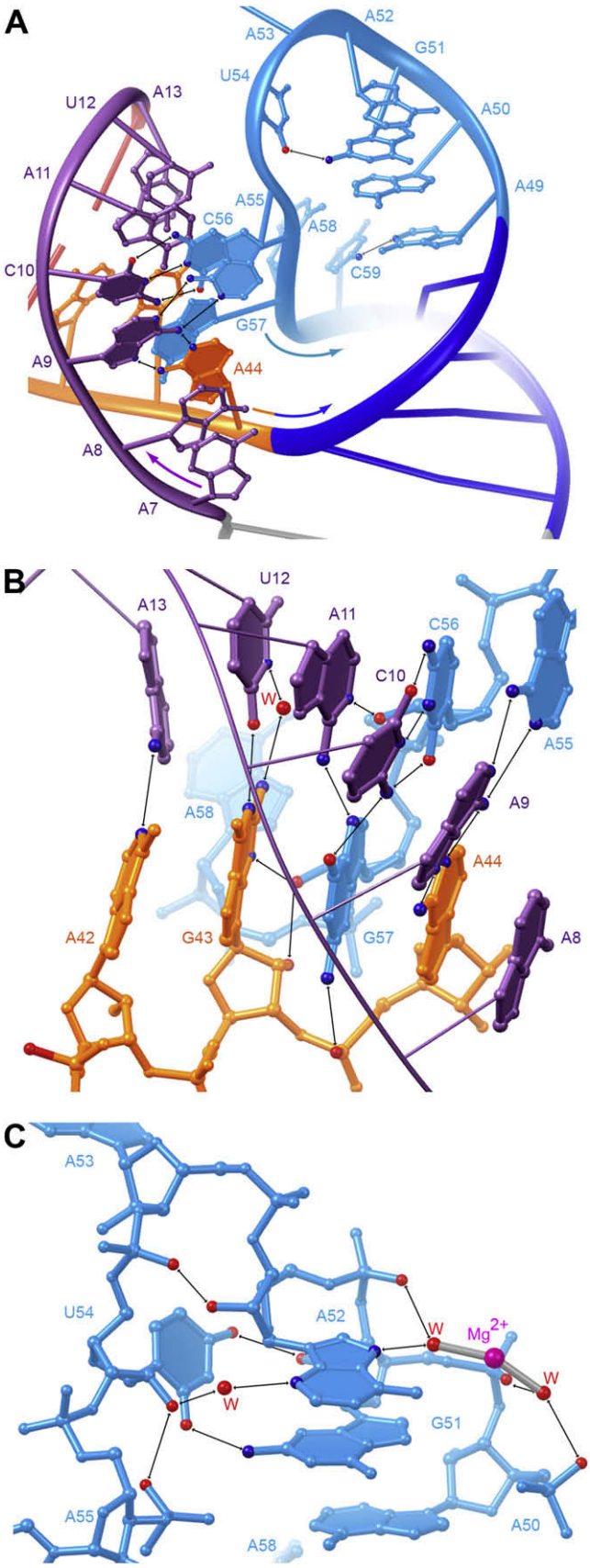

Figure 2. Structure of the Aptamer Core

(A) Interaction of L3 with the minor groove of the irregular helix formed by J1/2 and J2/3. Two-headed arrows denote selected hydrogen bonds.

(B) Structure of the core triplex. View is approximately perpendicular to that of (A).

(C) Detail of the top of L3. A well-ordered cation with two crystallographically resolved coordination waters and a water molecule bridging N3 of A52 and 2′-OH of U54 are shown. View is approximately that of (A).

Color coding as in Figure 1.

One makes one inner-sphere coordination with the *pro*-S_P phosphate of A44, while the other makes inner-sphere coordinations with the *pro*-S_P phosphate of A7 and the *pro*-R_P phosphate of A8. Both of these magnesium ions have octahedral coordination geometry, but one of the ligands of each (presumably water) is invisible in our current electron density maps.

DISCUSSION

Tetracycline Recognition

Studies in the Schroeder (Berens et al., 2001) and Suess (Müller et al., 2006) laboratories using tetracycline analogs demonstrated that the aptamer requires the hydroxyl group at position 6β of the antibiotic for binding. Thus, doxycycline (5-[α]-hydroxy-6-[β]-deoxytetracycline) binds the RNA with 150-fold lower affinity. This is not due to the 5-OH group present in doxycycline but absent from tetracycline, because the affinity of 5-(α)-hydroxytetracycline for the aptamer is only 2.3-fold lower than that of tetracycline. Our structure shows that 6β-OH is recognized through two hydrogen bonds by A13, whereas the 5 position of tetracycline points away from the binding pocket (Figure 3). The interaction of A13 with the 6β-OH of tetracycline was predicted through a thermodynamic double-cycle analysis (Müller et al., 2006). Our structure elucidates the precise nature of this intermolecular interaction. In our structure, A13 makes another hydrogen bond with tetracycline: with its ribose O4′ to the nitrogen of the amide group at position 2 of tetracycline. Consistent with the importance of this interaction, Müller et al. (2006) found that 2-nitrilotetracycline bound the aptamer with 13-fold reduced affinity.

Tetracycline binds to the aptamer by stacking its rings C and D on the purine base of A58. Ring D is aromatic and planar, whereas ring C is not. Indeed, the critical hydroxyl group at position 6 projects above the plane of the ring. Müller et al. (2006) found that anhydrotetracycline, which has an aromatic ring C resulting from loss of the critical 6β-OH and an adjacent hydrogen, bound the aptamer only 4.5 times more weakly than the parental compound. This suggests that for this compound, loss of the hydrogen bonds made by the 6β-OH with A13 is compensated for by improved stacking with A58, due to a planar ring C and the methyl group at position 6 now being on the plane of rings C and D. Conversely, 6-deoxy-6-demethyl tetracycline (sancycline), which lacks both substituents at position 6 but retains the nonplanar ring C, bound the aptamer 29 times more weakly than tetracycline (Müller et al., 2006). The dimethylamine group at position 4α of tetracycline projects out of the binding pocket (Figure 3A). Not surprising, its replacement with hydrogen results in only 2.6-fold loss of affinity (Müller et al., 2006). Remarkably, combination of the loss of the dimethylamine and the 6β-OH (in the form of 4-de-[dimethylamino]-5-hydroxy-6-deoxytetracycline) results in

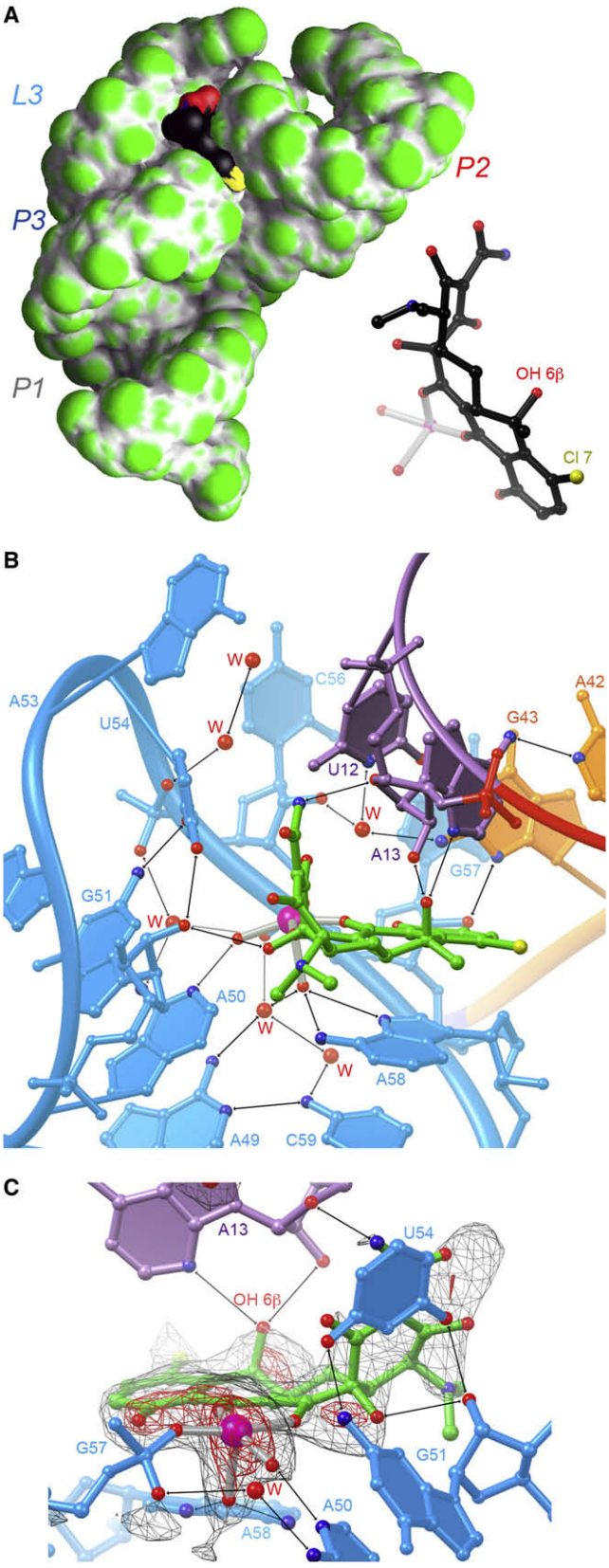

Figure 3. Structure of the Tetracycline Binding Site

(A) Solvent-accessible surface of the aptamer colored by curvature (green and gray are convex and concave, respectively) with a molecular surface representation of the bound 7-chlorotetracycline. In this panel only, carbon atoms of the antibiotic are drawn in black. Inset: ball-and-stick figure of the antibiotic and its coordinated, hydrated magnesium ion in the same orientation as in the surface representation. Note complete occlusion of the hydroxyl group at position 6β in the aptamer complex.

(B) Detail of the binding site.

(C) View of the binding site from the direction of L3, superimposed on the unbiased residual $|F_o| - |F_c|$ electron density into which the antibiotic-magnesium complex was built, contoured at 3 and 5 SD (gray and red mesh, respectively).

a 710-fold loss in affinity compared to tetracycline (Müller et al., 2006). This loss in affinity, which is considerably larger than that resulting from the loss of either the dimethylamine or the 6β-OH, suggests that this small molecule adopts a mode of binding distinctly different from that of the parental compound.

Tetracycline Binding-Induced RNA Structure

Hanson et al. (2005) extended the initial Pb^{2+} and DMS modification analyses of cb28 (Berens et al., 2001) by carrying out modification experiments using DMS, DEPC, CMCT, and kethoxal. These reagents probe for the exposure of nucleotide bases to bulk solution (reviewed in Brunel and Romby, 2000). A summary of the results obtained by Hanson et al. (2005) upon probing the tetracycline aptamer in the absence of the antibiotic are plotted on the RNA structure in Figure 5A. Excluding the modification at the distal end of P1 (due presumably to fraying of the helix), the sites of strong or intermediate modification are at the tip of L3, and in J1/2 and J2/3. Nucleotides G51, A52, and U54 of L3 are the most strongly modified positions. The high reactivity of the two purines is consistent with our cocrystal structure (Figure 2C), but not the reactivity of U54, because in the liganded structure of the RNA the uracil base is sequestered inside the L3. Thus, it appears that in the absence of the antibiotic, L3 is poorly folded. Nucleotides A7, A8, and A9 on one end of the triplex, and A42 and U12 on the other (cf. Figure 2B), display intermediate levels of modification. A7 and A8 are unpaired in our cocrystal structure, so their susceptibility to modification is expected. However, A9, U12, and A42 all participate in forming the triplex. Therefore, these results suggest that the core triplex of the aptamer is partially unfolded in the absence of antibiotic.

The change in susceptibility to modification of aptamer nucleotides by the same set of reagents between the free and tetracycline-bound states determined by Hanson et al. (2005) is plotted on the structure in Figure 5B. The largest changes occur in L3. Nucleotides A49, A50, G51, and U54 become markedly more protected upon tetracycline binding. This is consistent with L3 adopting the conformation displayed in our cocrystal structure, where U54 makes a bidentate interaction with the sugar (minor groove) edge of G51 (Figure 3C). The bases of A49 and A50 extend the 5′ strand of P3 by stacking on it (Figures 2A and 2C). G51 has been shown to crosslink to tetracycline when the complex is subjected to UV irradiation (Berens et al., 2001). As expected from its location directly underneath the bound tetracycline, nucleotide A58 becomes strongly protected. A55 and G57 from L3, both of which participate in formation of the core triplex, become moderately and strongly protected,

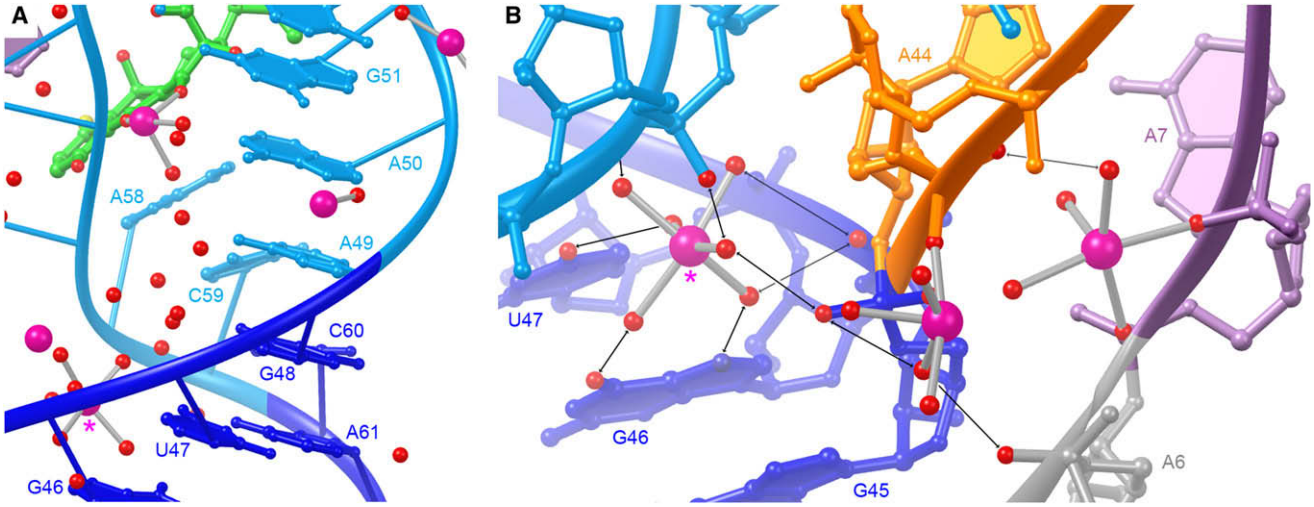

Figure 4. Water Molecules and Hydrated Magnesium Ions in the Aptamer-Tetracycline Complex

(A) Well-ordered water molecules fill the major groove of L3 linking the exterior of the complex with the α face of the antibiotic. View is from the rear of Figure 1D.

(B) Magnesium ions line the junction between the major groove of P3 and the backbones of J1/2 and J2/3.

Asterisks denote the same magnesium ion. Although all three magnesium ions have octahedral coordination geometry, only the crystallographically resolved ligands are shown.

respectively, in the presence of antibiotic. Four other nucleotides that form the core triplex, A9, U12, A13, and G43, also become moderately protected upon ligand binding. Although DMS is known to modify the N3 position of C (Brunel and Romby, 2000), neither C10 nor C56, which base pair with each other (Figures 2A, 2B, and 5C), are modified (Figures 5A and 5B). Because, in addition, these two cytosines are completely intolerant to mutation (Hanson et al., 2005), it appears that their Watson-Crick faces are engaged in base pairing even in the unbound aptamer. In summary, the modification experiments show asymmetry in that L3 nucleotides become strongly protected, whereas nucleotides of the irregular J1/2-J2/3 duplex become only moderately protected. Because the tetracycline binding pocket forms by association of L3 and the irregular duplex, this asymmetry in the degree of protection is striking. This is especially so in comparing the strong protection of G57, which interdigitates with nucleotides from J2/3 that are not as strongly protected.

Our cocrystal structure suggests the specific molecular nature of a tetracycline binding-induced rearrangement of the aptamer RNA that was initially proposed from biochemical probing studies (Berens et al., 2001; Hanson et al., 2005) and later elaborated on the basis of combined mutational and calorimetric analysis by Müller et al. (2006). The latter authors found that tetracycline binding to the cb28 minimer is strongly enthalpically driven (K_d = 0.77 nM; ΔH = −22.9 kcal/mol; $-T\Delta S$ = 10.5 kcal/mol). The A13U aptamer mutant bound tetracycline with a K_d of 222 nM. As would be expected from the multiple hydrogen bonds made between this nucleotide and the antibiotic in our structure, Müller et al. (2006) found that the loss in free energy of binding was primarily due to a decrease in favorable enthalpy (ΔH = −20.1 kcal/mol; $-T\Delta S$ = 11.0 kcal/mol). Our structure indicates that whereas a free U residue would be able to make the same interactions with the antibiotic as an A (with the O4 of U substituting for the hydrogen bond accepting N3 of A), as part of the RNA chain, a uridine would be unable to reach the Watson-Crick face of A42 (Figure 2B) and at the same time bind the antibiotic. The A50U mutant suffers a comparable loss in free energy of binding (K_d = 196 nM) but its thermodynamic signature is completely different. For this mutant, ΔH was found to be −10.2 kcal/mol and $-T\Delta S$ was 1.0 kcal/mol; that is, the enthalpy of binding decreased dramatically, whereas the entropy of binding became much more favorable. The structure of the complex shows that the adenine base of A50 recognizes the magnesium ion that coordinates the tetracycline, and also helps position RNA residues that interact with the antibiotic-metal ion chelate (Figure 3C). A50 also stacks on top of the 5′-helical stack of P3. A uridine would be unable to make all these interactions, and this presumably leads to the decrease in favorable enthalpy of binding. On the other hand, the more favorable entropy of binding suggests that in the A50U mutant, the antibiotic does not interact with L3, which does not suffer losses in its degrees of freedom. A binding mechanism in which the L3 side of the tetracycline pocket undergoes considerable ordering but the J1/2-J2/3 side is partially pre-organized would be consistent with these experiments, and with the asymmetric decrease in solvent exposure noted above.

Structural Basis of Tetracycline Binding

Regression analysis of the free energy of RNA-small molecule interaction as a function of the burial of solvent-accessible surface area demonstrated a linear relationship of 19 cal/mol per Å^2 (Edwards et al., 2007). This relationship is analogous to that noted for protein interfaces (Eisenberg and McLachlan, 1986), and is remarkable in that it holds across RNAs of a wide range of sizes and distinctly different structures. Prominent exceptions to this linear trend were the RNAs, both natural and artificial, that bind to simple purines. The affinities of these RNAs for their ligands were too high to be accounted for exclusively by burial of solvent-accessible surface area. Because the purine-binding riboswitches completely envelop their cognate ligands, their

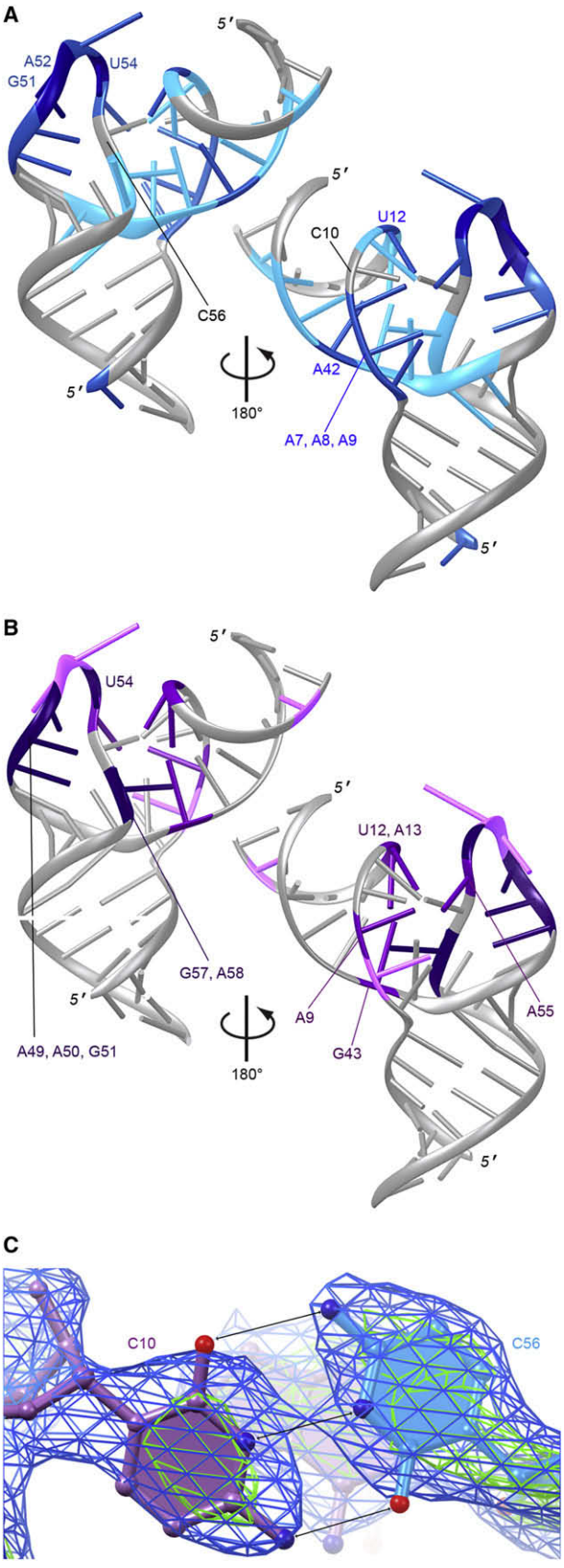

Figure 5. Biochemical Evidence for Tetracycline Binding-Induced Aptamer Reorganization

(A) Results of chemical probing of the unliganded aptamer by Hanson et al. (2005) plotted on the cocrystal structure. Dark, medium, and light blue denote most strongly, intermediate, and most weakly modified nucleotides, respectively.

(B) Magnitude of the change in chemical modification between the unliganded and liganded tetracycline aptamer, determined by Hanson et al. (2005) plotted on the crystal structure. Nucleotides with the largest changes are denoted by deep purple, intermediate changes by magenta, and smallest by pink.

(C) Portion of the experimental electron density (Fourier synthesis calculated with the density-modified MAD phases) corresponding to the C10•C56 *trans* Watson-Crick pair contoured at 1 and 3 SD (blue and green mesh, respectively) superimposed on the final crystallographic model.

high affinity likely arises from favorable RNA-RNA interactions that occur only concomitant with ligand binding.

The solvent-accessible area of tetracycline buried by binding to the cb28 minimer (425 Å^2) is insufficient to account for its subnanomolar dissociation constant. Ultimately, structural characterization of the unbound aptamer will be required to describe fully the molecular basis of tetracycline recognition. Nonetheless, our complex structure and previous biochemical studies suggest that, in addition to L3 folding, formation of the intricate J1/2-J2/3 duplex contributes to the energetics of binding. A9 is the central nucleotide of the base triple formed between A55, A9, and A44 (Figure 2A). Its mutation to G results in impaired binding to tetracycline (K_d = 162 nM), an enthalpy of binding more favorable, and an entropy of binding even more unfavorable, than for the wild-type (ΔH = −28.4 kcal/mol; $-T\Delta S$ = 19.7 kcal/mol). In contrast, mutation to G of A55, the third member of the base triple, minimally perturbs the affinity (K_d = 1.7 nM) or the enthalpically driven nature of binding (ΔH = −21.8 kcal/mol; $-T\Delta S$ = 10.6 kcal/mol) (Müller et al., 2006). The discrepancy in the effects of mutation of A9 or A55 is consistent with the J1/2-J2/3 duplex being partially prestructured. We suggest that reorganization of the former (induced by the A9G mutation) is entropically costly, whereas rearrangement of the precise interaction between the duplex and L3 (resulting from the A55G mutation) is not (compared to wild-type), because L3 folding and tetracycline binding are concomitant.

Solvent and ion fixation concomitant with RNA folding and tetracycline binding is evident in our cocrystal structure (Figure 4). The presence of highly ordered water networks in the interior of complexes of aptamers or riboswitches with their cognate ligands has been documented. For instance, the structure of the vitamin B_{12} aptamer-ligand complex shows evidence of water molecules that help stabilize noncanonical base pairing and facilitate burial of highly polarized molecular moieties (Sussman and Wilson, 2000). Thermodynamic analysis of hypoxanthine binding by the guanine riboswitch (Batey et al., 2004) demonstrated a highly enthalpically driven process (at 1.0 mM $MgCl_2$, K_d = 3 μM, ΔH = −35.4 kcal/mol, and $-T\Delta S$ = 27.6 kcal/mol). Crystallographic analysis of the riboswitch revealed that whereas the purine ligand is completely enclosed in the RNA, it remains partially solvated. Gilbert et al. (2006) proposed that the ability of the purine riboswitch to discriminate between closely related nucleobases rests on a strong dependence on hydrogen bonding, rather than base stacking, with the ligand. By surrounding the bound purine with water molecules, the

riboswitch in effect lowers the affinity for its ligand but increases its specificity. Our structure shows that in the case of the cb28-tetracycline interaction, stacking interactions are not the preponderant mechanism of recognition. Rather, the binding site is hydrated, and hydrogen bonding, for instance with the 6β-OH of tetracycline, is employed, allowing the RNA to achieve a high degree of selectivity.

Comparison with Other Tetracycline Binding Sites

An important motivation for the in vitro selection of aptamers against antibiotics is the elucidation of the range of molecular recognition strategies available to RNA (Lorenz and Schroeder, 2006). Comparison of our structure with the binding sites for tetracycline of the 30S subunit of the bacterial ribosome (Brodersen et al., 2000; Pioletti et al., 2001), TetR (Hinrichs et al., 1994), and elongation factor Tu (EF-Tu) (Heffron et al., 2006) shows that although all of these macromolecules recognize the magnesium ion chelate of the antibiotic, the specific combination of macromolecule-antibiotic interactions each employs is unique.

Tetracycline has a K_d of ~1 μM for the bacterial ribosome, and biochemical studies have mapped a functionally important binding site to the A site of the small subunit (Maxwell, 1967; Moazed and Noller, 1987). Several tetracycline binding sites are present in crystal structures of the tetracycline-bound 30S ribosomal subunit (Brodersen et al., 2000; Pioletti et al., 2001). The site of highest occupancy is at the A site, and is composed exclusively of ribosomal RNA (Figure 6A). The antibiotic is recognized primarily through its ketoenolate face through interactions with nonbridging phosphate oxygens and ribose 2′-OH groups. Although the hydration waters of the chelated magnesium ion are not resolved crystallographically, it appears that the ribosome also employs outer-sphere coordination to recognize the metal ion. Unlike the aptamer, which stacks with rings C and D of the antibiotic, the only stacking interaction in the primary site of the 30S subunit is a modest interaction with C1054. Interestingly, the 6β-OH that is critical for binding by the aptamer projects away from the rRNA. Indeed, there are no interactions between the ribosome and that face of the antibiotic, other than a possible electrostatic interaction between the tetracycline dimethylamine and the G966 phosphate. This sparse set of interactions is consistent with the comparatively low affinity of tetracycline binding to the ribosome.

Resistance to tetracycline by Gram-negative bacteria primarily results from export of the drug by an antiporter, TetA. The TetR protein regulates expression of TetA at the transcriptional level by releasing its operator when it binds the antibiotic. TetR is a dimeric DNA-binding protein in which the tetracycline binding site allosterically controls the orientation of the helix-turn-helix motif. Consistent with the high affinity (K_d ~1 nM) of TetR for its ligand (Takahashi et al., 1986), the protein completely envelops the antibiotic (Hinrichs et al., 1994; Kisker et al., 1995). The chelated magnesium ion makes an inner-sphere coordination with His100 from one protomer, and Glu147′ from the other subunit makes a bidentate outer-sphere interaction with two of the coordination waters of the metal ion (Figure 6B). Multiple hydrophobic side chains, including those of Arg104, Pro105, Leu131, Ile 134, and Leu174′, pack against ring D. TetR employs a polar-aromatic interaction (Burley and Petsko, 1988) between Phe86 and the tetracycline OH group at the junction of rings A and B. Finally, TetR makes an intricate network of hydrogen bonds with the polar groups that decorate ring A of the antibiotic, using side chains such as those of His64 and Asn82.

Both TetR and cb28 have an absolute requirement for Mg^{2+} for binding to the antibiotic. This stems from recognition of the metal ion chelate of the antibiotic by both macromolecules, and the need for counterions for folding of the RNA. Although inner-sphere coordination with the magnesium ion (through His100 and the nonbridging phosphate oxygen of G57 for TetR and the aptamer, respectively) is highly favorable, making this interaction in aqueous solution requires desolvation of the ion. Therefore, the net free energy gain from these interactions is likely modest (Draper, 2004). Outer-sphere interactions, on the other hand, need not overcome the enthalpy of solvation of Mg^{2+} and, if multidentate, have the additional entropic advantage stemming from the chelate effect. Both macromolecular complexes display this type of interaction (Glu147′ and A58 for TetR and the aptamer, respectively). Beyond the expected differences between a protein and an RNA, there are several noteworthy differences between the specific tetracycline features recognized by these two molecules. One is that the orientation of the antibiotic relative to the binding site is approximately reversed: ring A of tetracycline is most deeply buried in TetR, whereas it is partially solvent exposed in the aptamer. Another is that whereas the 6β-OH of tetracycline is essential for recognition by the aptamer, it is in fact detrimental for TetR-tetracycline interaction. Indeed, the side chain of Val113 clashes with this hydroxyl group (Hinrichs et al., 1994), and its removal results in 35-fold tighter binding to the protein (Degenkolb et al., 1991).

Riboswitch Function of the Tetracycline Aptamer

The discovery of riboswitches has given new impetus to the design of their artificial counterparts: RNAs that enable small-molecule control of gene expression in vivo. Although many aptamers to small molecules have been selected in vitro, only a handful have been found to function in vivo (reviewed in Suess and Weigand, 2008). Indeed, in vivo selection experiments suggest that features required for function within cells are underrepresented among aptamers, and an approach that combines in vitro selection to obtain aptamers and in vivo selection for gene-regulatory function offers promise. Unlike the neomycin (Weigand et al., 2008) and theophylline (Lynch et al., 2007) aptamers, which had to be optimized by in vivo selection to function efficiently, the tetracycline aptamer achieved control of gene expression essentially in its original form (Hanson et al., 2003; Suess et al., 2003; Weigand and Suess, 2007).

What are the molecular correlates of the ability of the tetracycline aptamer to function in vivo? There are three features of the tetracycline aptamer that are reminiscent of natural riboswitches. First, the affinity of the tetracycline riboswitch for its cognate ligand is comparable to that of the most stable natural riboswitch-effector interaction. Presumably, the affinities of natural riboswitches are tuned to the intracellular concentration of their effectors. Thus, the high affinity of cb28 for tetracycline, although important (Hanson et al., 2005; Müller et al., 2006), is unlikely to be key to its in vivo function. (Because of the difference in translation initiation mechanisms between eukaryotes and bacteria, it is possible that high affinity is more important in eukaryotes. However, the tetracycline aptamer cannot be tested in

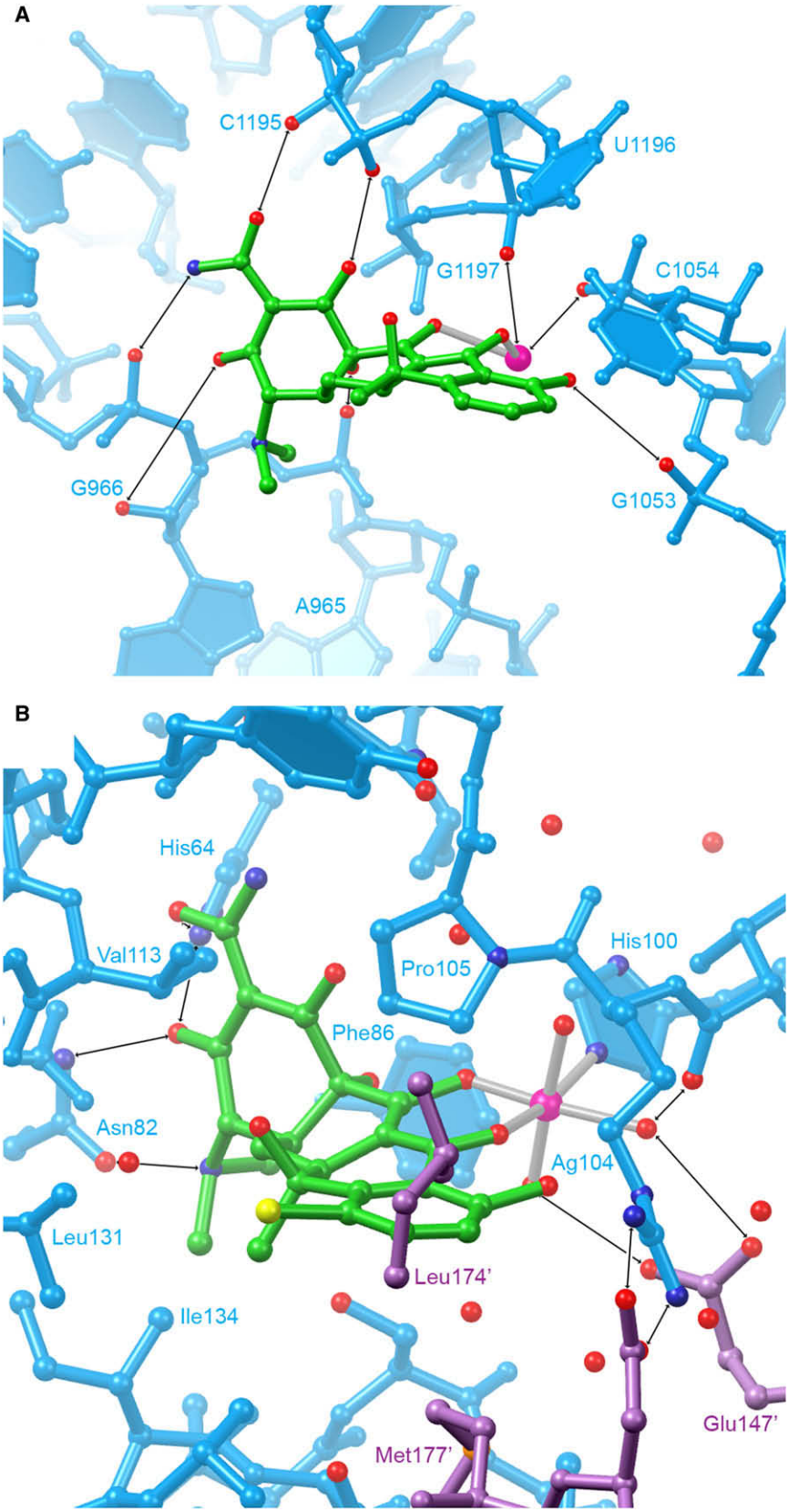

Figure 6. Comparison of Ribosomal and Protein Tetracycline Binding Sites

(A) Detail of the primary tetracycline binding site in the 3.4 Å resolution cocrystal structure of the 30S ribosomal subunit of *Thermus thermophilus* (Brodersen et al., 2000).

(B) Detail of the ligand binding site of the 2.1 Å resolution structure of the complex between the class D tetracycline repressor protein (TetR) and 7-chlorotetracycline (Hinrichs et al., 1994; Kisker et al., 1995). The binding site is formed by amino acid residues from both protomers of the dimeric protein. Amino acid residues from the second protomer are colored magenta.

bacteria because its ligand is an antibiotic.) Second, similarly to natural riboswitches such as the thiamine pyrophosphate-binding *thi* box and the glucosamine-6-phosphate-binding *glmS* ribozyme-riboswitch (Edwards et al., 2007), the tetracycline aptamer employs magnesium ion as a molecular handle to augment its ligand and recognize it indirectly. Although this mechanism is clearly advantageous for a negatively charged nucleic acid to bind to phosphate-containing metabolites, or the anionic ketoenolate moiety of tetracycline, natural riboswitches have evolved to function by recognizing neutral ligands such as guanine or adenine, or positively charged effectors such as S-adenosylmethionine. Thus, the use of chelated magnesium ions for recognition of effectors does not appear to be a requirement for in vivo function. Third, the overall architecture of the tetracycline riboswitch is reminiscent of that of several natural riboswitches in that it is composed of two helical stacks that pack together using long-range interactions, and cradle the ligand in their interface. A correlate of this architecture is the folding of some RNA regions concomitant with ligand binding. Thus, the purine riboswitch has an h-shaped architecture, harbors its ligand at the junction of three helices, and the binding reaction is strongly unfavorable entropically (Gilbert et al., 2006). Crystallographic analysis of the *thi* box (another h-shaped riboswitch) binding to ligands that span a 5000-fold range in affinity demonstrated progressive ordering of parts of the RNA with increasing affinity (Edwards and Ferré-D'Amaré, 2006). Blouin and Lafontaine (2007) have shown that a ligand binding-induced long-range loop-loop interaction of the lysine riboswitch is important for lysine-induced transcription termination. Thus, it is likely that the overall architecture and the ligand-induced local folding of the tetracycline riboswitch are important aspects of its ability to regulate gene expression in vivo.

SIGNIFICANCE

The tetracycline aptamer is unusual among in vitro selected small-molecule-binding RNAs because of its high affinity for its ligand, its three-helix junction architecture, and its ability to function as an artificial riboswitch. The crystal structure of the aptamer bound to 7-chlorotetracycline reveals a composite binding site at the junction of the two helical stacks of the h-shaped RNA. The aptamer appears to achieve high affinity and specificity by augmenting the antibiotic with a chelated magnesium ion, and by employing a binding site that does not rely exclusively on nucleobase stacking with the aromatic and conjugated rings of the antibiotic. In this, the binding site of the aptamer resembles that of the TetR protein (which binds tetracycline with an affinity similar to that of the aptamer). Interpretation of the results of previous biochemical and calorimetric analyses (Berens et al., 2001; Hanson et al., 2005) in light of our crystal structure suggests that localized folding of the binding site, and concomitant ordering of buried solvent and hydrated magnesium ions, accompanies antibiotic binding. This localized folding, and an overall h-shaped architecture stabilized by long-range interactions, make the tetracycline aptamer more similar to naturally occurring riboswitches, rather than to typical small-molecule-binding aptamers. The latter usually have simpler structures consisting of two stacked helices, and undergo large folding transitions upon binding their cognate ligand (Feigon et al., 1996; Hermann and Patel, 2000; Wilson and Szostak, 1999).

EXPERIMENTAL PROCEDURES

RNA and Protein Preparation

RNA was transcribed in vitro with T7 RNA polymerase from double-stranded DNA templates. These were generated by PCR using a 3′ primer containing two 2′-OMe nucleotides at its 5′ end to reduce 3′ heterogeneity of runoff transcripts (Kao et al., 1999). Transcription reactions (310K, 2 hr) contained 1/10 volume of PCR reaction, 30 mM Tris-HCl (pH 8.1), 30 mM $MgCl_2$, 0.01% (v/v) Triton X-100, 2 mM spermidine hydrochloride, 5 mM each of the four NTPs, 1 mM DTT, and 0.05 g/l T7 RNA polymerase. Reactions also contained 1 unit/ml of *Escherichia coli* inorganic pyrophosphatase (Sigma) to increase RNA yield (Rupert and Ferré-D'Amaré, 2004). RNA was purified by denaturing PAGE, passively eluted into water, washed with 1 M KCl, desalted and concentrated by ultrafiltration, and stored at 277K. Selenomethionyl U1A-RBD double mutant preparation has been described (Ferré-D'Amaré and Doudna, 2000a). The competition binding assay (Figure S1) was performed under conditions described by Müller et al. (2006).

Crystallization and Diffraction Data Collection

A solution comprising 0.3 mM RNA, 0.33 mM selenomethionyl U1A-RBD double mutant, 50 mM Tris-HCl (pH 7.5), 5 mM $MgCl_2$, 0.5 mM 7-chlorotetracycline, and 0.25 mM spermine hydrochloride was incubated for 20 min at 310K. Drops prepared by mixing 1 μl each of this solution and a reservoir solution comprising 50 mM HEPES-KOH (pH 7.0), 20 mM $MgCl_2$, and 12.5%–15% (w/v) PEG 8000 were equilibrated by vapor diffusion at 296K in the dark. Cube-shaped crystals with the symmetry of space group $P42_12$ (a = 120.84 Å; c = 55.28 Å; one RNA-U1A-chlorotetracycline complex per asymmetric unit) appeared within 4 weeks and grew over the course of 2 additional weeks to maximum dimensions of 0.15 mm^3. Crystals were transferred over the course of 10–15 min to a solution comprising 50 mM HEPES-KOH (pH 7.0), 20 mM $MgCl_2$, 15% (w/v) PEG 8000, 0.5 mM spermine hydrochloride, 0.5 mM 7-chlorotetracycline, and 30% (v/v) glycerol, mounted on nylon loops, and flash-frozen by plunging into liquid nitrogen. Three-energy MAD diffraction data were collected from a single crystal at beamline 5.0.2 of the Advanced Light Source (ALS, Lawrence Berkeley National Laboratory) and reduced with the HKL package (Otwinowski and Minor, 1997). Crystallographic statistics appear in Table 1.

Structure Determination and Refinement

Three selenium sites were located using the program SOLVE (Terwilliger and Berendzen, 1999). Heavy-atom parameters were refined, phases were calculated, and density modification was performed using the program CNS (Brünger et al., 1998). The resulting experimental electron density map was of excellent quality (Figure 5C) and allowed unambiguous building of the RNA, protein, and most of the RNA-bound magnesium ions and their coordination waters using the program O (Jones et al., 1991). Although clear electron density for the antibiotic was present, it was not included in the crystallographic model until near the end of refinement. Rounds of simulated annealing, energy minimization, and restrained isotropic atomic temperature factor refinement using a maximum-likelihood target with experimental phase probability distributions in CNS produced a model with R_{free} = 28.2%. The 7-chlorotetracycline was then placed into the residual electron density (Figure 3C), and final rounds of refinement were carried out with REFMAC (Murshudov et al., 1997) using a maximum-likelihood target and no TLS refinement (Figure S4). The final model comprises all RNA residues, U1A RBD residues 6–95, one 7-chlorotetracycline, 12 magnesium ions, and 146 water molecules. The β and γ phosphates of the 5′-triphosphate of the RNA lack electron density, are presumed disordered, and are not included in the crystallographic model. Refinement statistics appear in Table 1. Solvent accessibility was calculated with CNS, using a probe radius of 1.4 Å. Figures were prepared with Ribbons (Carson, 1997) and GRASP (Nicholls et al., 1993).

ACCESSION NUMBERS

Atomic coordinates and structure factor amplitudes of the tetracycline aptamer RNA in complex with 7-chlorotetracycline and the U1A RBD have been deposited in the Protein Data Bank under ID code 3EGZ.

SUPPLEMENTAL DATA

Supplemental Data include four figures and Supplemental References and can be found with this article online at http://www.chembiol.com/cgi/content/full/15/10/1125/DC1/.

ACKNOWLEDGMENTS

We thank the staff at ALS beamline 5.0.2, and J. Bolduc for assistance with synchrotron and in-house X-ray data collection, respectively, and T. Hamma, C. Hoang, D. Klein, N. Baird, J. Pitt, J. Posakony, and A. Roll-Mecak for discussions. T.E.E. was a Damon Runyon Fellow, and A.R.F.-D. is a Distinguished Young Scholar in Medical Research of the W.M. Keck Foundation and an Investigator of the Howard Hughes Medical Institute. This work was supported by grants from the Damon Runyon Cancer Research Foundation (DRG-1844-04 to T.E.E.) and the W.M. Keck Foundation (to A.R.F.-D.).

Received: July 1, 2008
Revised: August 28, 2008
Accepted: September 2, 2008
Published: October 17, 2008

REFERENCES

Batey, R.T., Gilbert, S.D., and Montange, R.K. (2004). Structure of a natural guanine-responsive riboswitch complexed with the metabolite hypoxanthine. Nature *432*, 411–415.

Berens, C., Thain, A., and Schroeder, R. (2001). A tetracycline-binding RNA aptamer. Bioorg. Med. Chem. *9*, 2549–2556.

Blouin, S., and Lafontaine, D.A. (2007). A loop-loop interaction and a K-turn motif located in the lysine aptamer domain are important for the riboswitch gene regulation control. RNA *13*, 1256–1267.

Brodersen, D.E., Clemons, W.M., Jr., Carter, A.P., Morgan-Warren, R.J., Wimberly, B.T., and Ramakrishnan, V. (2000). The structural basis for the action of the antibiotics tetracycline, pactamycin, and hygromycin B on the 30S ribosomal subunit. Cell *103*, 1143–1154.

Brunel, C., and Romby, P. (2000). Probing RNA structure and RNA-ligand complexes with chemical probes. Methods Enzymol. *318*, 3–21.

Brünger, A.T., Adams, P.D., Clore, G.M., Gros, P., Grosse-Kunstleve, R.W., Jiang, J.-S., Kuszewski, J., Nilges, M., Pannu, N.S., Read, R.J., et al. (1998). Crystallography and NMR system: a new software system for macromolecular structure determination. Acta Crystallogr. D Biol. Crystallogr. *54*, 905–921.

Burley, S.K., and Petsko, G.A. (1988). Weakly polar interactions in proteins. Adv. Protein Chem. *39*, 125–192.

Carson, M. (1997). Ribbons. Methods Enzymol. *277*, 493–505.

Degenkolb, J., Takahashi, M., Ellestad, G.A., and Hillen, W. (1991). Structural requirements of tetracycline-Tet repressor interaction: determination of equilibrium binding constants for tetracycline analogs with the Tet repressor. Antimicrob. Agents Chemother. *35*, 1591–1595.

Draper, D.E. (2004). A guide to ions and RNA structure. RNA *10*, 335–343.

Edwards, T.E., and Ferré-D'Amaré, A.R. (2006). Crystal structures of the *thi*-box riboswitch bound to thiamine pyrophosphate analogs reveal adaptive RNA-small molecule recognition. Structure *14*, 1459–1468.

Edwards, T.E., Klein, D.J., and Ferré-D'Amaré, A.R. (2007). Riboswitches: small-molecule recognition by gene regulatory RNAs. Curr. Opin. Struct. Biol. *17*, 273–279.

Eisenberg, D., and McLachlan, A.D. (1986). Solvation energy in protein folding and binding. Nature *319*, 199–203.

Ellington, A.D., and Szostak, J.W. (1990). In vitro selection of RNA molecules that bind specific ligands. Nature *346*, 818–822.

Feigon, J., Dieckman, T., and Smith, F.W. (1996). Aptamer structures from A to ζ. Chem. Biol. *3*, 611–617.

Ferré-D'Amaré, A.R., and Doudna, J.A. (2000a). Crystallization and structure determination of a hepatitis delta virus ribozyme: use of the RNA-binding protein U1A as a crystallization module. J. Mol. Biol. *295*, 541–556.

Ferré-D'Amaré, A.R., and Doudna, J.A. (2000b). Methods to crystallize RNA. In Current Protocols in Nucleic Acid Chemistry, S.L. Beaucage, D.E. Bergstrom, G.D. Glick, and R.A. Jones, eds. (New York: John Wiley & Sons), pp. 7.6.1–7.6.10.

Ferré-D'Amaré, A.R., Zhou, K., and Doudna, J.A. (1998a). A general module for RNA crystallization. J. Mol. Biol. *279*, 621–631.

Ferré-D'Amaré, A.R., Zhou, K., and Doudna, J.A. (1998b). Crystal structure of a hepatitis delta virus ribozyme. Nature *395*, 567–574.

Gilbert, S.D., Stoddard, C.D., Wise, S.J., and Batey, R.T. (2006). Thermodynamic and kinetic characterization of ligand binding to the purine riboswitch aptamer domain. J. Mol. Biol. *359*, 754–768.

Hanson, S., Berthelot, K., Fink, B., McCarthy, J.E., and Suess, B. (2003). Tetracycline-aptamer-mediated translational regulation in yeast. Mol. Microbiol. *49*, 1627–1637.

Hanson, S., Bauer, G., Fink, B., and Suess, B. (2005). Molecular analysis of a synthetic tetracycline-binding riboswitch. RNA *11*, 503–511.

Heffron, S., Mui, S., Aorora, A., Abel, K., Bergmann, E., and Jurnak, F. (2006). Molecular complementarity between tetracycline and the GTPase active site of elongation factor Tu. Acta Crystallogr. D Biol. Crystallogr. *62*, 1392–1400.

Hermann, T., and Patel, D.J. (2000). Adaptive recognition by nucleic acid aptamers. Science *287*, 820–825.

Hinrichs, W., Kisker, C., Düvel, M., Müller, A., Tovar, K., Hillen, W., and Saenger, W. (1994). Structure of the Tet repressor-tetracycline complex and regulation of antibiotic resistance. Science *264*, 418–420.

Jones, T.A., Zou, J.Y., Cowan, S.W., and Kjeldgaard, M. (1991). Improved methods for building protein models in electron density maps and the location of errors in these models. Acta Crystallogr. A *47*, 110–119.

Kao, C., Zheng, M., and Rüdisser, S. (1999). A simple and efficient method to reduce nontemplated nucleotide addition at the 3′ terminus of RNAs transcribed by T7 RNA polymerase. RNA *5*, 1268–1272.

Kisker, C., Hinrichs, W., Tovar, K., Hillen, W., and Saenger, W. (1995). The complex formed between Tet repressor and tetracycline-Mg^{2+} reveals mechanism of antibiotic resistance. J. Mol. Biol. *247*, 260–280.

Leontis, N.B., and Westhof, E. (2001). Geometric nomenclature and classification of RNA base pairs. RNA *7*, 499–512.

Lorenz, C., and Schroeder, R. (2006). Aptamers to antibiotics. In The Aptamer Handbook, S. Klussmann, ed. (Weinheim, Germany: Wiley-VCH Verlag), pp. 116–130.

Lynch, S., Desai, S., Sajja, H., and Gallivan, J. (2007). A high-throughput screen for synthetic riboswitches reveals mechanistic insights into their function. Chem. Biol. *14*, 173–184.

Maxwell, I.H. (1967). Partial removal of bound transfer RNA from polysomes engaged in protein synthesis in vitro after addition of tetracycline. Biochim. Biophys. Acta *138*, 337–346.

Moazed, D., and Noller, H.F. (1987). Interaction of antibiotics with functional sites in 16S ribosomal RNA. Nature *327*, 389–394.

Müller, M., Weigand, J.E., Weichenrieder, O., and Suess, B. (2006). Thermodynamic characterization of an engineered tetracycline-binding riboswitch. Nucleic Acids Res. *34*, 2607–2617.

Murshudov, G.N., Vagin, A.A., and Dodson, E.J. (1997). Refinement of macromolecular structures by the maximum-likelihood method. Acta Crystallogr. D Biol. Crystallogr. *53*, 240–255.

Nicholls, A., Bharadwaj, R., and Honig, B. (1993). GRASP: graphical representation and analysis of surface properties. Biophys. J. *64*, A116–A125.

Otwinowski, Z., and Minor, W. (1997). Processing of X-ray diffraction data collected in oscillation mode. Methods Enzymol. *276*, 307–326.

Pioletti, M., Schlünzen, F., Harms, J., Zarivach, R., Glühmann, M., Avila, H., Bashan, A., Bartels, H., Auerbach, T., Jacobi, C., et al. (2001). Crystal structures of complexes of the small ribosomal subunit with tetracycline, edeine and IF3. EMBO J. *20*, 1829–1839.

Pleij, C.W. (1990). Pseudoknots: a new motif in the RNA game. Trends Biochem. Sci. *15*, 143–147.

Rupert, P.B., and Ferré-D'Amaré, A.R. (2004). Crystallization of the hairpin ribozyme: illustrative protocols. Methods Mol. Biol. *252*, 303–311.

Suess, B., and Weigand, J.E. (2008). Engineered riboswitches—overview, problems and trends. RNA Biol. *5*, 24–29.

Suess, B., Hanson, S., Berens, C., Fink, B., Schroeder, R., and Hillen, W. (2003). Conditional gene expression by controlling translation with tetracycline-binding aptamers. Nucleic Acids Res. *31*, 1853–1858.

Sussman, D., and Wilson, C. (2000). A water channel in the core of the vitamin B_{12} RNA aptamer. Structure *8*, 719–727.

Takahashi, M., Altschmied, L., and Hillen, W. (1986). Kinetic and equilibrium characterization of the Tet repressor-tetracycline complex by fluorescence measurements. Evidence for divalent metal ion requirement and energy transfer. J. Mol. Biol. *187*, 341–348.

Terwilliger, T.C., and Berendzen, J. (1999). Automated MAD and MIR structure solution. Acta Crystallogr. D Biol. Crystallogr. *55*, 849–861.

Weigand, J.E., and Suess, B. (2007). Tetracycline aptamer-controlled regulation of pre-mRNA splicing in yeast. Nucleic Acids Res. *35*, 4179–4185.

Weigand, J.E., Sanchez, M., Gunnesch, E., Zeiher, S., Schroeder, R., and Suess, B. (2008). Screening for engineered neomycin riboswitches that control translation initiation. RNA *14*, 89–97.

Welz, R., and Breaker, R. (2007). Ligand binding and gene control characteristics of tandem riboswitches in *Bacillus anthracis*. RNA *13*, 573–582.

Wilson, D.S., and Szostak, J.W. (1999). In vitro selection of functional nucleic acids. Annu. Rev. Biochem. *68*, 611–647.